



**Fermi National Accelerator Laboratory**

**FERMILAB-Pub-87/178-E**

**[E-741/CDF]**

## **Phototube Testing for CDF\***

**T. Devlin, J. Cruz<sup>(a)</sup>, U. Joshi, K. Kazlauskis,  
C. Muehleisen, T.-S. Yang<sup>(b)</sup>**

**Department of Physics and Astronomy, Rutgers - The State University  
P.O. Box 849, Piscataway, New Jersey 08854**

**J. E. Elias, H. Jensen**

**Fermi National Accelerator Laboratory  
P.O. Box 500, Batavia, Illinois 60510**

**L. Nodulman**

**Argonne National Accelerator Laboratory  
Argonne, Illinois 60431**

**July-August 1987**

**\*Submitted to Nucl. Instrm. Methods A**



**Operated by Universities Research Association Inc. under contract with the United States Department of Energy**

DRAFT 1 July 1987

Phototube Testing for CDF

by

T. Devlin, J. Cruz,<sup>(a)</sup> U. Joshi, K. Kazlauskis,

C. Muehleisen, T.-S. Yang<sup>(b)</sup>

Department of Physics and Astronomy, Rutgers - The State University

P. O. Box 849, Piscataway, New Jersey 08854

J.E. Elias, H. Jensen,

Fermilab, P. O. Box 500, Batavia, Illinois 60510

L. Nodulman

Argonne National Laboratory, Argonne, Illinois 60431

ABSTRACT

Photomultiplier tubes for the Collider Detector at Fermilab were subjected to pre-installation testing for stability, linearity and other properties. An apparatus is described which provided computer control of light sources, monitoring of environmental conditions and data logging of responses from up to 48 photomultiplier simultaneously. Statistical summaries of the test results are included for 1041 tubes for the central electromagnetic calorimeter and 687 tubes for the endwall hadron calorimeter.

(To be submitted to Nuclear Instruments and Methods)

## I. INTRODUCTION

The central electromagnetic calorimeter system for the Collider Detector at Fermilab was designed to detect and measure the energy of photons, electrons and positrons emerging from proton-antiproton collisions at 2 TeV. The system, described in detail elsewhere [1], consists of 480 towers surrounding the intersection region in a projective geometry. Each tower consists of 30 layers of 0.32-cm-thick lead and 31 layers of 0.50-cm-thick scintillation plastic, a total of 18 radiation lengths. Light from the scintillators is brought out each end by Y7 doped UVA acrylic wavelength shifters (wavebars) to two photomultiplier tubes (PMT's) per tower.

This system has an energy resolution  $\Delta E/E = 14\%/\sqrt{E}$ , where the energy, E, is expressed in GeV. Since interesting physics is expected in the region where E is 100 GeV or more, it is necessary for this system to operate at a level of 1% accuracy. The problems of calibration, stability, linearity and uniformity are formidable.

To minimize potential problems, the phototubes and bases in this system were subjected to extensive pre-installation testing to ensure that each of them met specifications, to establish operating characteristics and to exercise each for approximately one week to monitor stability and detect early failures.

A total of 1041 tubes (Hamamatsu Model R580B) and bases were tested for the central EM calorimeter. In addition, another 687 tubes (Thorn-EMI Model 9902KB06) and bases for the end wall hadron calorimeter [2] were subjected to similar, but briefer tests in the same apparatus.

This paper briefly describes the apparatus and procedures used for these tests and summarizes the results. A more detailed description can be obtained elsewhere.[3]

## II. APPARATUS AND PROCEDURES

### A. Test Overview

This section describes the testing program for the Hamamatsu R580B selected for the central electromagnetic calorimeters. A number of the requirements for the photomultipliers, such as geometry and spectral sensitivity, were automatically met by the selection of tube type. The manufacturer provided measurements of quantum efficiency (QE) over a specified spectral range of green light appropriate to the wave bars (see Fig. 2.1.), and all tubes delivered were above the specified 8% minimum value. Statistics on the distribution of QE's for the tubes are given in Table 2.1 along with other results discussed in subsequent sections. Our tests had three main goals which are listed below.

1. Establishing the DC supply voltages corresponding to three fixed operating points for the product of gain (G) times QE. The nominal setting was  $1.2 \times 10^4$  (e.g. a gain of  $10^5$  for a tube with QE = 12%), and at twice and four times that amount.
2. Eliminating tubes with early failures or substandard performance characteristics by exercising each one for approximately 160 hours while continuously monitoring the pulse response linearity, gain stability and rate effects. The first 40 hours of this exercise were devoted to a "burn-in" period with roughly 5  $\mu$ Amps of anode current in each tube.

3. Measuring specific characteristics using subsamples of the tubes in order to verify acceptable calorimetry performance. These included temperature dependence of the G•QE product, gain recovery time after a single large pulse, and useful lifetime.

The number of tubes to be tested in a period of about one year available before the first CDF run clearly required automated test procedures and data acquisition for many tubes simultaneously. Our approach was to use standard CAMAC control and data acquisition modules interfaced to S-100 bus system Z80 microcomputers with a link to a remote VAX 11/780 computer for data logging and subsequent analysis. The microcomputers provided the stand-alone capability needed for ease of hardware interfacing, test fixture development and calibration.

Two types of test fixtures were constructed for these measurements: a small, single-tube test chamber for initial inspection, operating voltage determination and dark current measurements; and a pair of identical 24-tube test chambers for the long-term repetitive testing cycles.

Upon receipt of tubes from the manufacturer in monthly batches of 100, the set of initial, semi-automated tests were performed using the single-tube fixture. Approximately 15 minutes per tube was required. At this point, the data bases for groups of forty tubes (plus eight controls which remained resident in the large test chambers) were started with the manufacturer's data and these test results, and the forty tubes were installed in the main test

facility. After initial setup by the operator, the large-chamber tests and data logging were fully automatic for 160 hours.

## B. Single-Tube Test Fixture

The initial testing, to establish operating voltages at each of three gain settings, and to measure dark current, was performed in a small, single-tube chamber. Figure 2.2 shows the functions of this apparatus schematically. The light-tight test chamber contained a single LED and a sleeve-and-stop assembly which guided each PMT photocathode into a fixed position relative to the LED. An S-100 based, Z80 microcomputer ( $\mu\text{C}$ ) provided operator guidance through various steps in the test and logged the results on floppy disks for use in subsequent tests and the PMT database. The  $\mu\text{C}$  was equipped with an interface to a CAMAC crate where the integrating analog-to-digital converter (ADC) and some control circuitry were located.

Clock-driven NIM logic modules provided pulses with fixed charge to drive the LED, and a gate signal for the ADC. The output of the PMT could be plugged into the ADC for pulse-area measurements, or into a pico-ammeter for dark current measurements.

The voltage for each tube was manually adjusted to yield a standard pulse response to the test chamber LED. The amplitude was chosen in the following manner. The earliest tubes delivered were measured by the manufacturer to have QE's from 8% to 16% with an average of 12%. At several voltage settings, their absolute current gains were measured as described in Section II-D, and they were set to gains of  $1.0 \times 10^5$ . These tubes were then used as "bootstraps" for a standard response in the single-tube chamber with their photocathodes in a fixed position relative to the LED. The voltage for every subsequent tube was adjusted to give a fixed pulse area corresponding to a  $G \cdot \text{QE}$  product of  $1.2 \times 10^4$ , i.e. a gain of  $10^5$  for a QE of 12%. Two other voltage settings were also determined for  $G \cdot \text{QE}$ 's of  $2.4 \times 10^4$  and  $4.8 \times 10^4$ .

At this stage, each tube was fitted with a base [4] which remained with it permanently if the combination was accepted. Voltages and associated dark currents for each each tube-base assembly at each of the above operating points were recorded on floppy disks for use in subsequent tests. If an assembly failed to meet specifications, its tube and base were each checked in other combinations to isolate and reject the inferior component. Essentially all of the roughly 2% tube failures were for excessive dark current detected at this stage. Some sparking problems detected in early deliveries of the bases were eliminated by changes in the construction procedures.

For purposes of interpolation between measured points, the dependence of gain,  $G$ , on voltage,  $V$ , was parametrized as follows:

$$\langle G_i/G_j \rangle = \langle V_i/V_j \rangle^N. \quad (2.1)$$

The distributions of the voltage settings, the associated dark currents and the values of  $N$  for the tubes tested are described in Table 2.1.

### C. Large Test Chambers

A diagram of the major features of the main test facility is given in Fig. 2.3. A second Z80  $\mu$ C in an S-100 bus system was used as a front end controller interfaced to CAMAC. It was connected by an asynchronous line to a VAX 780 for data logging. The Z80 controlled the sequence of DC and pulsed light source tests, and the PMT high voltage. It recorded data from the ADC's which read pulsed response of the tubes, anode currents, power supply voltages and temperatures. The two test chambers described below were capable of handling a combined total of 48 tubes, 40 under test and 8 long term controls. At peak rate, we followed a weekly cycle of 160 hours testing plus 8 hours for exchanging tubes for the next cycle. Various features of the apparatus and procedures are listed below.

The principal geometric features of the test chambers are shown in Fig. 2.4. Two such top-loading, light-tight chambers were built, each holding 24 tubes supported in a 5x5 lattice (central position empty). Each position in the lattice contained a magnetic shield, plastic leaf springs and a stop to position the photocathode in a reproducible fashion.

#### 1. Light Sources

The main bank of light sources (Table 2.2) was located on the wall of the chamber 70 cm from the photocathodes. The sources were mounted on four identical printed circuit boards placed symmetrically on that wall to smoothe the illumination profile at the bank of photocathodes. Each individual phototube was illuminated by four additional LED's placed on the support lattice approximately 3 cm from each photocathode to provide high amplitude

pulsed signals. A light map at the photocathode positions was measured with one of the sources which provided about  $3000 \text{ pe}^-$  at the center of the lattice.

The array of pulsed green LED's was organized into nine groups, each with a fixed illumination levels as indicated in Table 2.2. For stability, the pulse light sources were driven by a current pulse and were flashed at a  $\sim 10$  Hz rate which never varied during a test. "On" and "off" states were achieved by phase selection, i.e. changing the timing of the pulse by  $\sim 2 \mu\text{sec}$  relative to the 800-nsec-wide ADC gate. The typical pulse was roughly triangular with a width of  $\sim 150 \text{ ns}$  at 10% of full amplitude. The maximum PMT output amplitude with combined light levels 6 through 9 was  $\sim 15 \text{ mA}$ .

It should be emphasized that the absolute number of photons incident on the photocathodes from the LED's was neither known nor absolutely determined. Linearity measurements were based on data from a set of redundant, phase-selected combinations of light sources, subjected to statistical tests of the linearity hypothesis. Stability tests, after corrections for measured temperature dependence, assumed that the LED's remained stable over a period of one week.

Small tungsten filament lamps driven by digital-to-analog converters (DAC's) were used as steady light sources which could be set to produce anode currents ranging from  $20 \text{ nA}$  to  $>5 \mu\text{A}$ .

## 2. Analog-to-Digital Converters

The ADC used for pulse area measurements was the LeCroy 2285A, a 15-bit integrating ADC with a least count of  $\sim 0.03 \text{ pC}$ , corresponding to  $\sim 2 \text{ pe}^-$  at a tube gain of  $10^5$ , and a full range of  $>20,000 \text{ pe}^-$ . This covered the operating range expected in the detector. Some tests at  $>15 \text{ mA}$  peak pulsed current were

done with a  $\times 5$  attenuator at the ADC input. Two calibration methods were used for each of the 48 channels (see Ref. 3), and they agreed to 1% with a linearity of better than 1%.

A Dual Systems Model AIM-12 ADC residing on the S-100 bus was used to measure various low-level DC power supply voltages, the output voltages from temperature sensors [3] and anode currents. Each phototube output was sent to a  $\mu\text{C}$ -controlled reed-relay which could direct the anode signal to the LeCroy ADC or a multi-range current-to-voltage amplifier. When required, the tubes were switched, one at a time, to the amplifier, whose output was digitized by the Dual Systems ADC.

### 3. High Voltage Control and Readout

High voltage, including regulation and readout, for the 48 phototubes under test was supplied by a LeCroy 1440 system controlled by the  $\mu\text{C}$  through CAMAC. Values were automatically set to those specified in the database by the single-tube tests.

#### D. Test Cycle and Data Analysis

The main emphases of the test cycle and data analysis were stability, rate sensitivity and linearity. After the burn-in period, the  $\mu\text{C}$  executed a set of nested loops for 100 hours at the voltage settings corresponding to  $G \cdot QE = 1.2 \times 10^4$ . The outer loop cycled over the four settings of the tungsten lamp (Table 2.2). At each setting, it executed a stability test, a linearity test, and read out the anode currents, temperature sensors and various voltages. The stability test consisted of 500 readings (in ~50 seconds) each of pedestal (all pulsed levels off), and individual pulsed levels 1 through 6. Only means and RMS deviations were logged to the Vax. The linearity test consisted of 100 readings (in ~10 seconds) each of pedestal and fifteen different combinations of the same six pulsed light levels. Again, only means and RMS deviations for the 100-pulse sample were retained. The latter permitted a six-parameter fit to a linearity hypothesis for fifteen pieces of data.

In Fig. 2.5(a) the mean ADC response to pulsed Level 6 in the stability test is plotted as a function of time starting after the burn-in period. The change in pulsed response between the lowest and highest level for the tungsten lamp (Table 2.2) is clearly seen in the ~0.5% displacement between the two sets of points. Fig. 2.5(b) shows the output of the temperature sensors which varied diurnally by about  $4^\circ\text{C}$ . The phototube shows a clear change in output which is about -0.3% per degree-C, and is a combination of the measured change in LED output ( $-0.66\%/^\circ\text{C}$ ) and the tube response. Approximately 12 hours of data were lost by an overnight interruption in the VAX link, but the testing continued uninterrupted.

Additional results on the absolute gains, temperature dependence and relative quantum efficiencies were also obtained. The absolute gain for pulsed signals in each phototube is the ratio of the charge collected at the anode to the charge reaching the photocathode. The anode charge was measured by the absolute calibration of the ADC's described briefly above. Gain estimates based on single  $pe^-$  pulse-area measurements were impractical. Instead, the number of  $pe^-$ ,  $P$ , was determined from the ratio of the mean pulse area,  $H$ , (determined from 500 samples) to the standard deviation,  $\sigma$ , of the pulse area distribution:

$$\left[\frac{\sigma}{H}\right]^2 = \frac{1}{P} + b \quad (2.2)$$

where the first term,  $1/P$ , accounts for  $pe^-$  statistics, and  $b$  represents non-statistical contributions to the width of the pulse-area distribution. This relationship was tested by varying  $P$  with neutral-density filters. The results indicate that  $b \approx 10^{-5}$  or less. Since our gain measurements are based on pulsed light levels yielding no more than 20,000  $pe^-$  ( $1/P > 5 \times 10^{-5}$ ), the procedure can be valid at the 20% level or better for a stable system. The value of  $P$  yields the gain through the relationship

$$G = \frac{H}{eP} \quad (2.3)$$

Our experience with the full body of test data tended to support the validity of this procedure. However, two successive runs of the test chambers (out of thirty for the central EM tubes), while satisfactory in all other respects,

show spuriously large gains for all tubes including the controls. These runs were omitted from any distributions which involve this calculation.

Since the absolute number of photons incident on the photocathodes was unknown, we were unable to measure the absolute quantum efficiency of the tubes under test, but values relative to the sample average were calculable. This involved corrections for the variation of the light intensity with position in the test chamber lattice, and changes in light intensity after repairs on the test chambers. Details are given in [3]. Correlations between this measured relative quantum efficiency and the manufacturer's value were made.

### III. RESULTS: CENTRAL EM PHOTOTUBES

#### A. Full Sample Tests

##### 1. Dependence on Time, Temperature and Anode Current

The data for each tube and pulsed light source were fit to a time-dependent function with the following form:

$$H(t) = a_1 + a_2t + a_3t^2 + a_4[T(t) - T(0)] \quad (3.1)$$

where the a's are fitted parameters, t is the time (starting with t = 0 at the end of the 40-hour burn-in period), T(t) is the measured temperature as a function of time. This was done for each pulse level and DAC setting for the tungsten lamp which controls the anode current.

##### 2. Short-Term Stability

The stability criterion was met if, after unfolding the temperature dependence, the minimum-to-maximum variation (or "peak-to-peak drift") of the residual time dependence was less than 2%. A small number of tubes (<1%) marginally exceeded this criterion. They were re-cycled through the entire test, including a second burn-in period, and none was ultimately rejected for this reason. Table 2.1 describes the distribution of the measured variation.

##### 3. Current Gain

Table 2.1 describes the distribution of gains obtained by the method described in Section II-D. Also given are statistics on the pulse area,

corrected for position and time variations of the pulsed light intensity. This is proportional to the product  $G \cdot QE$ , and indicates that the tubes were all tested at quite uniform settings for this quantity as intended. In fact, the width of this distribution is dominated by uncertainties in the correction procedure rather than setting error.

#### 4. Temperature Dependence

In order to isolate the separate variation of the LED and phototube responses with temperature, the chamber was temporarily equipped with a glass separator and heaters to induce large ( $\sim 20^{\circ}\text{C}$ ) and independent changes in the temperatures at the LED and phototube volumes of the chamber. The LED temperature coefficient was  $-(0.66 \pm 0.03)\%/^{\circ}\text{C}$ .

Measurements of the environmental temperature variations were included in the normal test procedure, and the analysis yielded the combined temperature dependence of both the LED output and phototube response, viz.  $a_4$  in Eq. (3.1). The precision of individual determinations varied greatly, depending on the magnitude of the ambient temperature changes. Nevertheless, selecting only the more precise results made little difference in the average phototube/base temperature coefficient, only a slight narrowing of the distribution was observed. The result listed in Table 2.1 is drawn from the full sample, after correcting for the measured LED coefficient.

#### 5. Rate Effects

The rate dependence was tested by observing the change in pulse area as a function of average anode current controlled by the tungsten lamp. Figure 3.1 shows a scatter plot of the percentage change in pulse area vs. anode current. It is quite stable from a the 10 nA level arising from the LED's up to about 3

$\mu\text{A}$  where it abruptly rises. The stable region covers all normal conditions expected in CDF operation.

## 6. Linearity

The technique used for linearity testing was chosen to avoid any dependence on the long term stability of light sources or filters at the 1% level. The PMT response was measured for each of fifteen different combinations of up to three pulsed LED's levels 1 through 6. The combinations were: 1, 1+2, 1+2+3, 2, 2+3, 2+3+4, 3, 3+4, 3+4+5, 4, 4+5, 4+5+6, 5, 5+6, and 6. These combinations covered a dynamic range from typically  $\sim 30$  to  $>10,000$   $\text{pe}^-$ , with 10% to 30% increments about the largest single level in each combination. If the response is linear, the measured pulse areas should be well-represented by the appropriate linear combinations of six parameters, one amplitude for each of the six LED levels used. A  $\chi^2$  test with nine degrees of freedom can be made for such a fit. For higher values of the pulse area, H, the statistical uncertainty,  $\Delta H$ , was well below 0.1%. Therefore, since the specifications called for 1% linearity, a lower limit of 1% of H was placed on  $\Delta H$  for purposes of the  $\chi^2$  test.

Data for the fifteen different combinations of LED's required about seven minutes to collect, and the test was repeated about twice per hour for the duration of the testing period. All  $\chi^2$ 's were averaged to give a single value for each PMT, and the statistics on the averages is given in Table 2.1. The distribution is as expected for a linearity of 1% or better, viz.  $\chi^2 \approx 9$ .

## B. Subsample Tests

### 1. Pulse Recovery

Pulse recovery was defined to be satisfactory if the tube current gain recovered to within 2% of its previous value within 1 ms after a full-scale pulse (40 mA peak). An argon flash lamp was set up to provide this large pulse followed, with variable delay, by a smaller pulse from an LED. A change in the tube output pulse area for this delayed pulse was assumed to be due to a change in tube gain because of the large preceding pulse. With a 10  $\mu$ sec delay, a 4% rise in pulse area was observed, but at 100  $\mu$ sec or greater, there was no detectable effect on the pulse area.

### 2. Differential Linearity (Flash Lamp Tests)

The flash lamp, LED setup described in the previous section was operated with zero delay to test differential linearity at large amplitude. The output signal was attenuated by  $\times 11.3$  to bring it into the ADC range, and pulse areas were measured for the combination, LF, and each source individually L and F. A measure of percentage differential non-linearity is

$$D = \left( \frac{LF - F}{L} - 1 \right) \times 100\%. \quad (4.3)$$

The flash lamp yielded  $F = 500,000 \text{ pe}^-$  and the four highest amplitude LED's provided  $L = 80,000 \text{ pe}^-$ . This tested amplitudes well beyond the expected operating range of CDF. Eighteen tubes were tested in this manner. Half yielded  $D < 1\%$ , and the worst case was 5%. It is fairly easy to show that, if the non-linearity is a low order term in a power series (e.g. a quadratic

term), even the worst case implies integral non-linearities well under 1% in the range of interest.

### 3. Long Term Stability

Eight tubes and bases, including four R580B's remained in the test chambers as controls throughout the duration of the testing program, about thirty months. The total integrated current passing through these tubes reached about fifty coulombs. Conditions were far from stable because the high voltage was switched off every time a new batch of forty tubes was installed, and the entire test setup was moved to a new location three times. Nevertheless, we attempted to study possible changes in gain over this period. There are indications that the R580B gains diminished fairly steadily to about 90% of their original values over this period. The estimated uncertainty is about 5%.

#### IV. ENDWALL CALORIMETER TUBES

The EMI phototubes for the endwall hadron calorimeter were subjected to tests similar to those described above. The tests differed in two respects: after 40 hours of burn in, the subsequent testing period was reduced to about 40 hours instead of 120; the tubes were operated at gains of approximately  $10^6$  instead of  $10^5$ . We chose not to change any characteristics of the test fixtures, e.g. the ADC conversion gains. As a result, the pulse response for light level 6 was often off scale for the EMI tubes.

The data analysis yielded the results summarized in Table 4.1. The most significant effect of the absence of data for light level 6 for most tubes is that the linearity tests for the EMI sample were done over a narrower dynamic range ( typically 70:1 ) than for the R580B's (typically 250:1). Thus, the smaller  $\chi^2$  values should not be interpreted as evidence for better performance.

The duration of the test period (less than two diurnal temperature cycles) yielded large measurement uncertainties and strong correlations between parameters for tests of stability and temperature dependence. The results are omitted from Table 4.1, but they are consistent with no drift and zero temperature coefficient with an uncertainty of about 2%. The variation of gain with anode current for the EMI tubes was quantitatively very similar to that for the Hamamatsu tubes as shown in Fig. 3.1.

## V. ACKNOWLEDGEMENTS

We would like to thank the following people for valuable contributions and suggestions: Robert Darling, Mark Devlin, Ted Devlin, Robert Plano, Lee Scott, Bob Stone, Alvin Tollestrup and Debbie Weiss. This work was supported in part by the National Science Foundation No. NSF-PHY-85-14193 and the U.S. Department of Energy Nos. W-31-109-ENG-38 and DE-AC02-76CH03000.

FOOTNOTES AND REFERENCES

- (a) Present address: I.T.T. Avionics, 390 Washington Av., Nutley, NJ 07011
- (b) Present address: Room 2B108, AT&T Bell Labs, 555 Union Blvd., Allentown, PA 18103
- [1] L. Balka et al., "The CDF Central Electromagnetic Calorimeter", (submitted to Nuclear Instruments and Methods).
- [2] S. Bertolucci et al., "The CDF Central and End Wall Hadron Calorimeters" (submitted to Nuclear Instruments and Methods).
- [3] T. Devlin et al., Fermilab Report CDF-502, Fermilab, Batavia, Ill., 1987.
- [4] The bases for the R580B photomultiplier tubes were designed and build at the University of Pennsylvania under the supervision of J. Cook and R. Van Berg. A circuit diagram can be found in Ref. 1.

## FIGURE CAPTIONS

Fig. 2.1 (A) Spectral sensitivity for the R580B phototube. (B) Output spectrum of Y7 waveshifters. (C) Output spectrum of the light source used by the manufacturer in quantum efficiency measurements. The peak in the overlap of (A) and (C) is at 510 nm indicated by arrow (D). The wavelength of the green LED's used in the present tests is 560 nm, indicated by arrow (E).

Fig. 2.2 Small test chamber for measuring operating points and dark currents.

Fig. 2.3 Large test chamber block diagram. The clock pulsed all the LED light sources at 10 Hz. The microcomputer selected which sources were "on" (within the ADC gate) or "off" (delayed beyond the ADC gate), and the steady light levels. The phototube outputs were normally all connected to the LeCroy ADC for pulse height measurements. Periodically, they were switched, one at a time, to an amplifier/ADC system which measured the average anode current. The same ADC also monitored low-level DC voltages for the light sources and the temperature in the test chambers. The photomultiplier high voltage supply was controlled by the microcomputer through CAMAC.

Fig. 2.4 The geometry of the large test chambers. The shaded areas of Section AA contained the the timing circuitry (located in the center) and four driver boards, each containing identical sets of circuitry for all pulsed light levels, 1-5, and a tungsten lamp.

Section BB contained 24 circular holes to pass light through to the photocathodes, approximately 3 cm to the right on this diagram. The shaded areas in BB supported driver circuitry for light levels 6-10 and the associated LED's which protrude into the apertures for each tube.

Fig. 2.5 A sample of data which shows the dependence of the pulse area response of one of the photomultipliers on time, temperature and average anode current. (a) The time dependence for a specific pulsed light source (yielding about 15000 photoelectrons per pulse). Data are shown for two different settings of the tungsten lamp which induced a DC current in the phototube (approximately 0 and 2  $\mu$ Amps). The tube gain increases about 0.5% for the higher current. (b) The temperature in the test chamber during the same period. The dependence of pulse area on temperature is seen - about  $-0.3\%/^{\circ}\text{C}$ .

Fig. 3.1 A scatter plot of the percentage change in pulse height as a function of anode current. The reference pulse height is that with the tungsten lamp off. Note the logarithmic scale on the current axis.

Table 2.1

## Characteristics of R580B Phototubes for Central EM Calorimeter

Quantity	Units	Sample Size	Distribution		Min. Value	Max. Value
			Mean	Std. Dev.		
Quantum Eff.	%	1041	14.1	1.6	8.0	19.0
HV1 (a)	Volts	1041	1057	55	920	1200
HV2 (a)	Volts	1041	1163	62	1020	1340
HV3 (a)	Volts	1041	1282	71	1120	1480
Gain-Voltage Exponent (N in Eq. 2.1)						
HV2/HV1	--	1041	7.25	0.18	6.4	7.8
HV3/HV2	--	1041	7.15	0.22	6.1	7.7
Log <sub>10</sub> (I <sub>d</sub> /1 nA) (b)						
@ HV1	--	1041	-1.02	0.51	-2.4	0.4
@ HV2	--	1041	-0.83	0.51	-2.2	0.6
@ HV3	--	1041	-0.58	0.53	-1.8	0.8

Quantities below are for the HV1 setting

Corrected Pulse Area (c)	pC	963	26.9	1.5		
Gain (d)	( $\times 10^5$ )	849	1.00	0.24		
$\chi^2$ (9 d.f.) for Linearity Test ( $\sigma > 1\%$ )	--	1041	9.8	4.1		
Temp. Coeff. (e)	%/°C	1041	0.4	0.6		
Peak-to-Peak Drift in Pulse Area (f)	%	865	-0.4	1.3		

## Notes:

- (a) HV1 is the high-voltage setting for a nominal gain of  $1.0 \times 10^5$ . HV2 and HV3 are the settings for twice and four times that value, respectively.

- (b) On a linear scale histograms for dark currents,  $I_d$ , were strongly skewed and peaked near zero. On a logarithmic scale, they were roughly Gaussian with the parameters given here.
- (c) Value for light level 5. The absolute pulse area is of no significance. The standard deviation of the distribution is a measure of our ability to correct for position and time variations of the pulsed light sources.
- (d) Average value which required at least two consistent measurements from light levels 4, 5 and 6. For this sample, the uncertainty on the average for an individual phototube was required to be  $<0.1 \times 10^5$ .
- (e) Corrected for  $-0.66\%/^{\circ}\text{C}$  variation of LED's.
- (f) Measured over  $\sim 80$  hours and corrected for temperature dependence. For each test chamber, several runs were omitted from this sample because they had large statistical uncertainties for three or more tubes (of 24). The uncertainties on individual measurements varied from 0.3% to 2%. The distribution width is consistent with measurement uncertainties, and there is no evidence for drifts at this level.

Table 2.2  
 Characteristics of Light Sources in Large Test Chambers

Level Number	Type	# of sources	Distance to PMT (cm)	Nominal Pulse <sup>(c)</sup> (photoelectrons)	Anode Current (nA)
1	Pulsed <sup>(a)</sup>	4	70	30	(b)
2	"	4	70	100	"
3	"	4	70	300	"
4	"	8	70	1,000	"
5	"	24	70	3,000	"
6	"	1 <sup>(d)</sup>	3	20,000	"
7	"	1 <sup>(d)</sup>	3	20,000	"
8	"	1 <sup>(d)</sup>	3	20,000	"
9	"	1 <sup>(d)</sup>	3	20,000	"
	Step- Function <sup>(a)</sup>	16	70	--	0-100
	Tungsten Lamps <sup>(e)</sup>	4	70	--	0-10,000

- Note:
- (a) Green LED's with wavelength of 560 nm.
  - (b) The average anode current from all nine pulsed light sources was about 10 nA.
  - (c) Actual numbers varied downward by as much as 50% depending on tube location and quantum efficiency.
  - (d) One LEDF for each phototube position.
  - (e) The tungsten filament lamps were set to yield ~5 $\mu$ A anode current during burn-in, and were cycled through four different settings for the stability tests: off, ~20 nA, ~200 nA, and ~2 $\mu$ A.

Table 4.1

## Characteristics of EMI Phototubes for Endwall Hadron Calorimeter

Quantity	Units	Sample Size	Distribution		Min. Value	Max. Value
			Mean	Std. Dev.		
Quantum Eff.	%	687	18.9	2.3	10.0	23.0
HV1 (a)	Volts	687	962	136	700	1280
HV2 (a)	Volts	687	1054	158	740	1420
HV3 (a)	Volts	687	1158	184	800	1580
Gain-Voltage Exponent (N in Eq. 2.1)						
HV2/HV1	--	687	7.74	0.71	5.4	9.4
HV3/HV2	--	687	7.59	0.78	5.6	9.8
Log <sub>10</sub> (I <sub>d</sub> /1 nA) (b)						
@ HV1	--	687	-0.16	0.43	-2.2	0.8
@ HV2	--	687	0.07	0.42	-2.0	1.0
@ HV3	--	687	0.34	0.42	-1.0	1.2

Quantities below are for the HV1 setting

Corrected Pulse Area (c)	pC	687	191	34
Gain (d)	( $\times 10^5$ )	550	9.54	3.58
$\chi^2$ ( 8 d.f.) for Linearity Test ( $\sigma > 1\%$ )	--	687	3.8	1.0

## Notes:

- (a) HV1 is the high-voltage setting for a nominal gain of  $1.0 \times 10^6$ . HV2 and HV3 are the settings for twice and four times that value, respectively.
- (b) On a linear scale the dark current histograms were strongly skewed and peaked near zero. On a logarithmic scale, they were roughly Gaussian with the parameters given here.
- (c) Value for light level 5. The absolute pulse area is of no significance. The spread is a measure of our ability to correct for position and time variations of the pulsed light sources.

- (d) Average value which required at least two consistent measurements from light levels 4, 5 and, when available, 6. For this sample, the uncertainty on the average for an individual phototube was required to be  $< 2 \times 10^5$ .

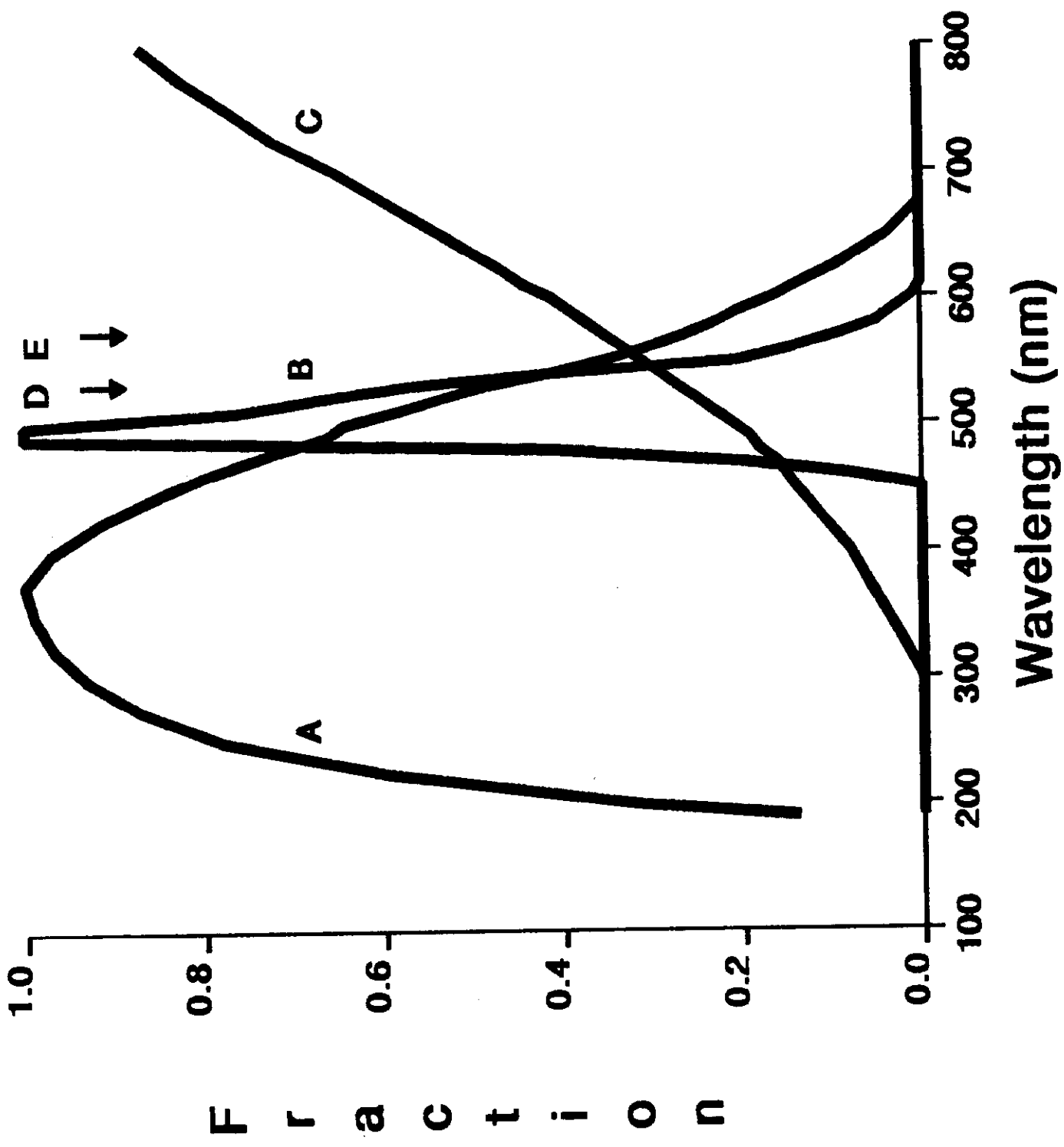
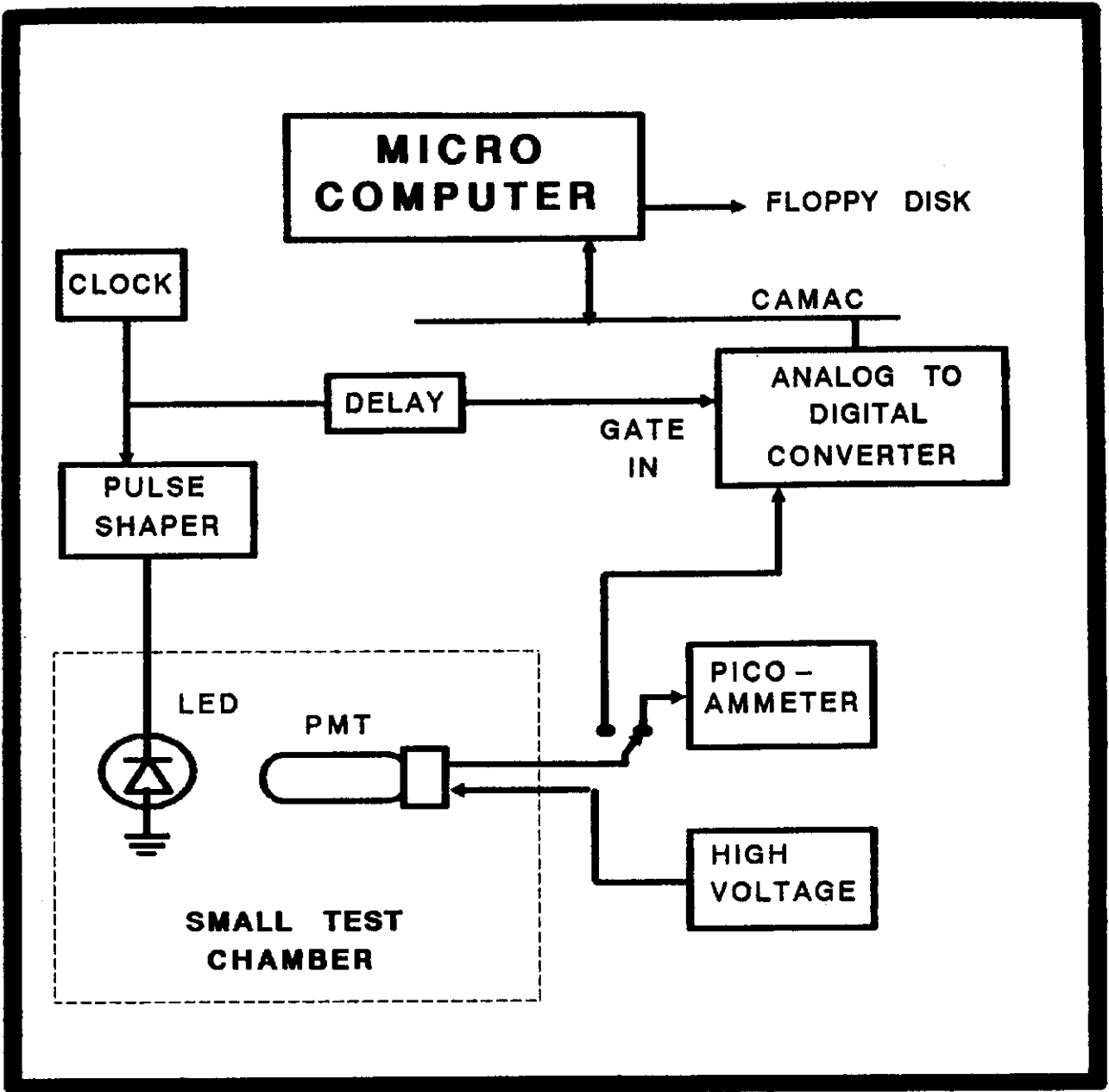


Fig 2.1



*Fig 2.2*

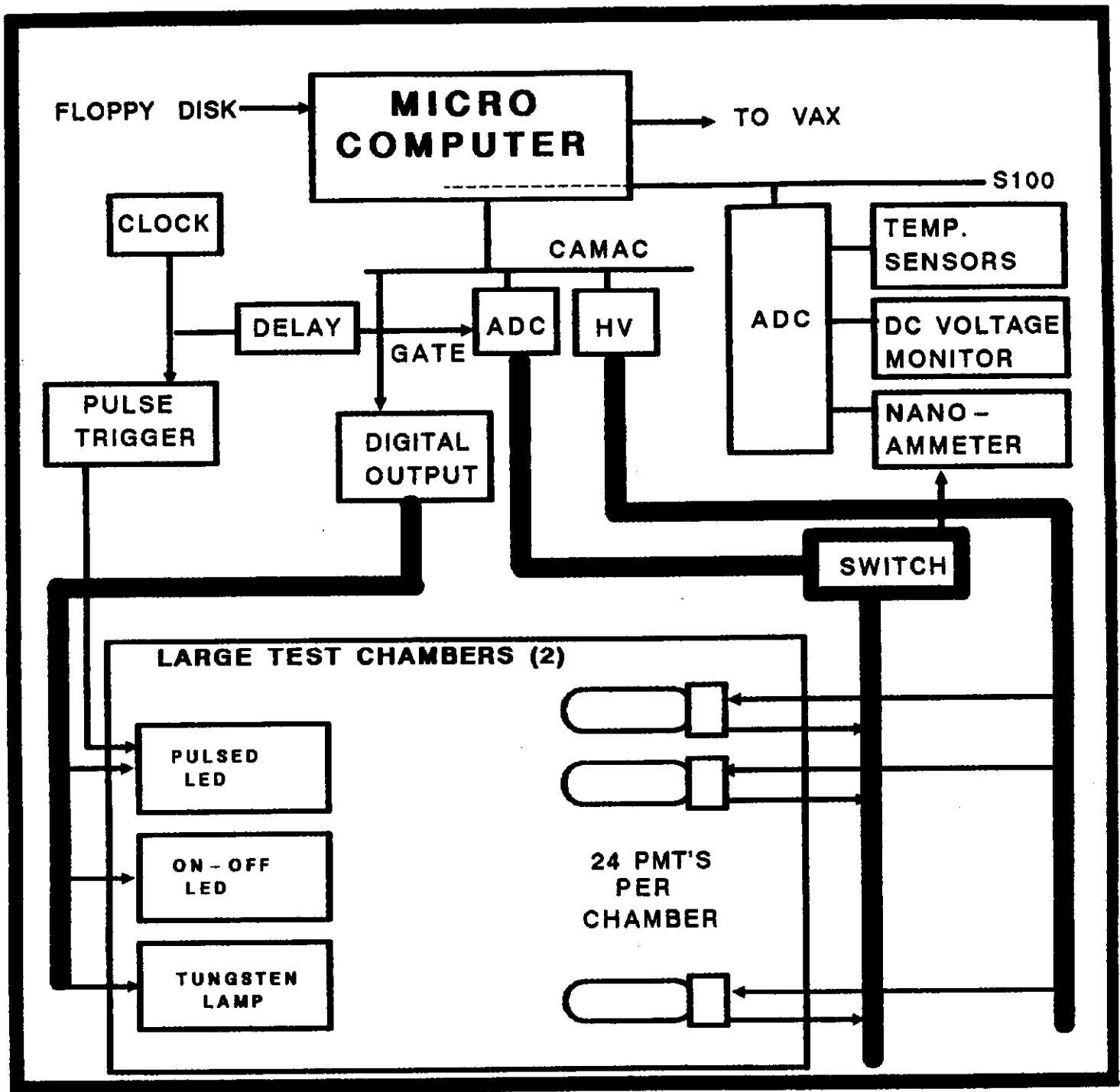


Fig. 2.3

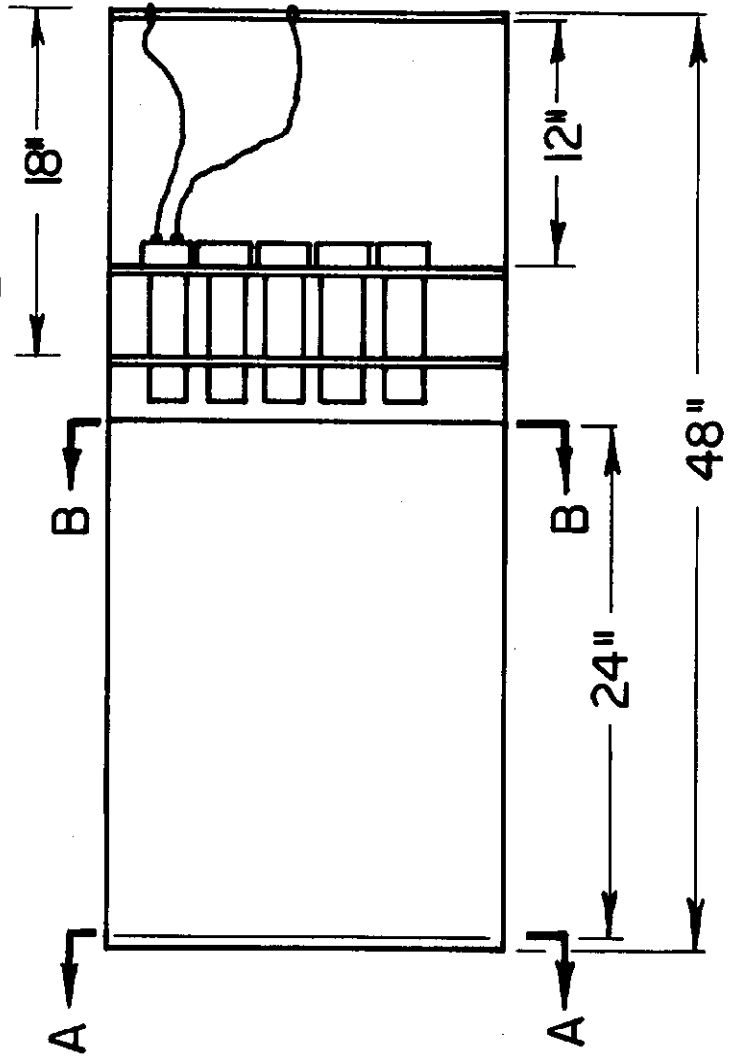
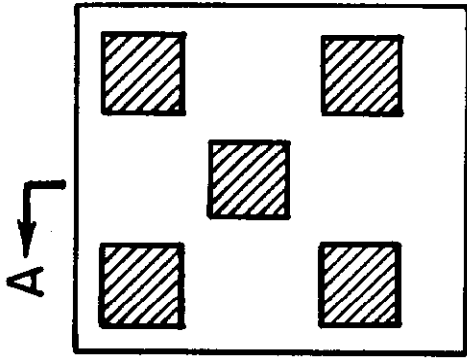
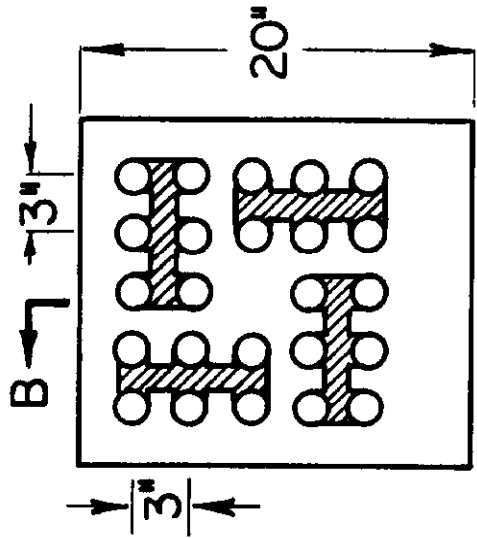
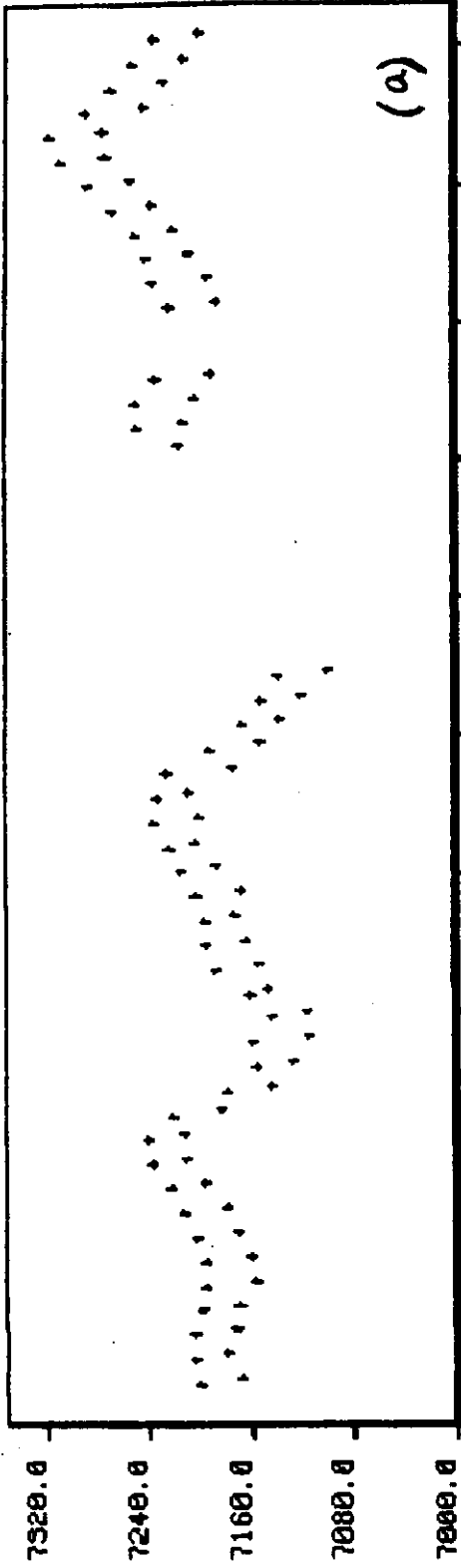
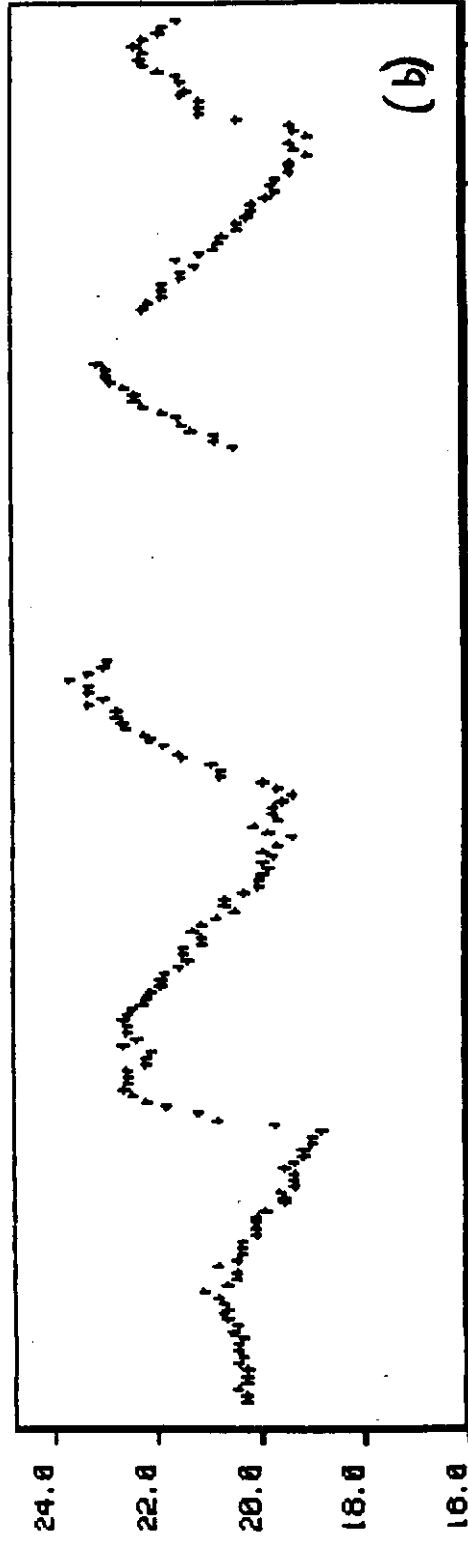


Fig. 2.4

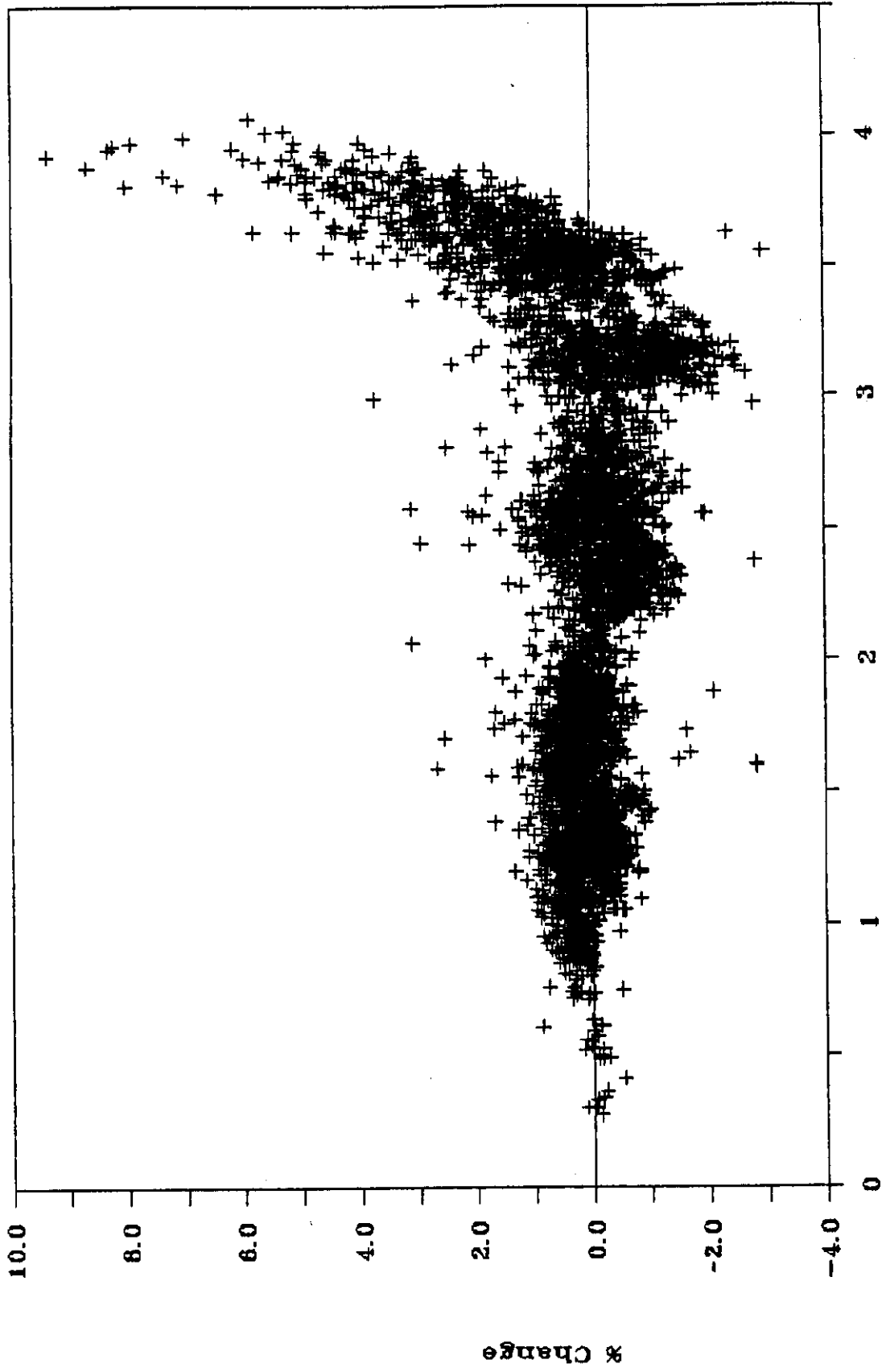


45.0 55.0 65.0 75.0 85.0 95.0 105.0 115.0 125.0 135.0 145.0  
 RB7059 PH-6 SLOT 21 VS HOURS SINCE 13:50:31 9/12/86



45.0 55.0 65.0 75.0 85.0 95.0 105.0 115.0 125.0 135.0 145.0  
 ENV T4 (DEGC) SLOT 0 VS HOURS SINCE 13:50:31 9/12/86

*Fig 2.5*



Log(Anode Current/1 nA)

*Fig 3.1*